SPANDIDOS PUBLICATIONS

EXPERIMENTAL AND THERAPEUTIC MEDICINE 12: 653-660, 2016

Dual-domain denoising in three dimensional magnetic resonance imaging

JING PENG, JILIU ZHOU and XI WU

Department of Computer Science, Chengdu University of Information Technology, Chengdu, Sichuan 610225, P.R. China

Received March 9, 2015; Accepted April 27, 2016

DOI: 10.3892/etm.2016.3345

Abstract. Denoising is a crucial preprocessing procedure for three dimensional magnetic resonance imaging (3D MRI). Existing denoising methods are predominantly implemented in a single domain, ignoring information in other domains. However, denoising methods are becoming increasingly complex, making analysis and implementation challenging. The present study aimed to develop a dual-domain image denoising (DDID) algorithm for 3D MRI that encapsulates information from the spatial and transform domains. In the present study, the DDID method was used to distinguish signal from noise in the spatial and frequency domains, after which robust accurate noise estimation was introduced for iterative filtering, which is simple and beneficial for computation. In addition, the proposed method was compared quantitatively and qualitatively with existing methods for synthetic and *in vivo* MRI datasets. The results of the present study suggested that the novel DDID algorithm performed well and provided competitive results, as compared with existing MRI denoising filters.

Introduction

Magnetic resonance imaging (MRI) is a medical imaging tool that can provide highly detailed images of tissues and organs in the human body (1,2). It is primarily used to demonstrate pathological and physiological alterations in living tissues (1,2), since it is non-invasive and can produce accurate three dimensional (3D) representations of internal structures of the human body (3). However, MRI images are easily contaminated by random noise, which limits the accuracy of quantitative measurements and the validity of diagnoses (4). Commonly used image denoising methods deal with Gaussian noise; however, denoising methods for MRI must be adapted for Rician noise MRI images provides a more accurate representation of information, which may benefit the denoising procedure (5).

Numerous MRI denoising approaches have been proposed by researchers. Sijbers *et al* (6,7) applied the maximum likelihood (ML) approach to reduce bias associated with the conventional denoising method, estimate the Rician noise and perform signal reconstruction. Conversely, in 2008, Aja-Fernandez *et al* (8,9) used the linear minimum mean square error estimator, in which the true value for each noisy pixel was estimated by a set of pixels selected from a local neighborhood. In addition, Wiener filtering is an adaptive optimal estimation method that uses the minimum mean square error as a criterion for denoising, and has been used to remove Rician noise in MRI (10).

Denoising in the spatial domain is the most direct approach. In 1985, Mcveigh *et al* (11) developed the spatial and temporal filters for reducing Gaussian noise in MRI images; however, both the noise and signal were reduced by the same factor and the signal-to-noise ratio (SNR) was unaffected. In 1990, Perona and Malik (12) established a multiscale smoothing scheme termed the anisotropic diffusion filter to overcome this defect; they smoothed markedly in the slow changing areas and suppressed at the boundaries by detecting the local gradient strengths in different directions in order to preserve the edges. In 2005, Buades *et al* (13) proposed the nonlocal means (NLM) filter, which uses the redundancy of patterns within the images to remove noise, and then adapted it for Rician noise correction in MRI (14,15). These local methods preserve the main structure and eliminate image blurring caused by subtle structures (15). However, as a result of the complexity of 3D MRI data, computational burden has emerged as a major challenge.

As well as denoising methods in the spatial domain, a number of methods, such as wavelet-based filers (16) and discrete cosine transform (17), are based on the processing of images in the transform domain. These approaches attempt to separate edge information from noise in the transform domain, and then remove noise while simultaneously preserving the edges and fine details (4). Denoising methods that are based on denoising patches, such as block matching with 3D filtering (BM3D) (18), which stacks the collected patches on top of one another and denoises them by 3D-wavelet shrinkage, have emerged as the most state-of-the-art image denoising methods in recent years (17). However, such methods are complex and thus prohibit a thorough analysis.

Knaus and Zwicker (19) developed a dual-domain image denoising (DDID) method that can produce high-quality results.

Correspondence to: Dr Xi Wu, Department of Computer Science, Chengdu University of Information Technology, 24 Block 1 Xuefu Road, Chengdu, Sichuan 610225, P.R. China
E-mail: xi.wu@cuit.edu.cn

Key words: three dimensional magnetic resonance imaging denoising, dual-domain denoising, robust noise estimation

In the present study, the DDID algorithm was adapted for a 3D MRI dataset with robust Rician noise estimation and 3D implementation in both the spatial and transform domains.

Data and methods

Algorithm. The present method for 3D MRI denoising was adapted from a recently proposed DDID algorithm for natural and synthetic images (20). Initially, a gradient descent was performed by progressively estimating Rician noise differentials and subtracting them iteratively from a noisy dataset. Subsequently, the noise differentials were estimated using robust kernels in both the spatial and frequency domains.

Noise removal by gradient descent. According to previous studies, a noise-free MRI image (x) will be corrupted by Rician noise (n) with zero mean and σ standard deviation (6,7). Hence, the noisy MRI dataset (y) may be represented as follows:

$$y = x + n$$

The denoising procedure may be regarded as an energy minimization problem for the optimal estimation of $n\hat{}$. Thus, the denoising procedure was formulated as a gradient descent, as follows:

$$x_i = x_{i+1} + \lambda \nabla E(x_i)$$

Where i is the number of iterations and λ is the scale factor that controls the step size in the direction of the gradient descent. The algorithm was initialed at $x_0=y$. The energy term $E(x_i)$ was then estimated as a noise estimate (λn_i) for iteration i, as follows:

$$x_i = x_{i+1} + \lambda n_i$$

This permitted the reinterpretation of the gradient descent as a progressive removal of noise differentials (λn_i), which was integrated over time (i) to estimate the total noise, as follows:

$$\hat{n} = \lambda \sum_{i=0}^{\infty} n_i$$

Robust noise estimation in dual-domains. To accomplish progressive noise removal, the noise for each iteration should be robustly estimated. In the DDID method, the noise was estimated via wavelet shrinkage, and denoising was performed by shrinkage of the wavelet coefficients in the wavelet domain to preserve the signal and to discard the noise (20). In the present study, the signal was considered the outlier and the noise as the inlier being estimated; the denoised signal was not estimated directly, but determined by subtracting the estimated noise. Noisy MRI images may be divided into three categories: Large amplitude signals, medium amplitude signals and small amplitude noise (19,20). Large amplitude signals, like step signals, have large gradients and are easily recognized and detected in the spatial domain. Signal and noise are uncorrelated when the signal and noise amplitudes are similar (i.e. medium amplitude signal). In the present study, medium amplitude signals were detected as large amplitudes in the frequency domain, thereby allowing the small amplitude noise to be estimated by rejecting the large amplitudes.

Signals should be distinguished from noise so as to compute the noise estimation (n_i) for iteration (i). Initially, the robust noise estimator for i was implemented in the spatial domain, where large amplitude signals were removed. Considering pixel p using pixels q in a neighborhood window N_p with window radius r, the gradient ($g_{i,p,q}$) was computed by subtracting the center pixel value ($x_{i,p}$) from all the neighboring pixels ($x_{i,p}$), as follows:

$$g_{i,p,q} = x_{i,q} - x_{i,p}$$

In this framework, the gradient was used to define a smoothly decaying range kernel (k_r), which masked large signals from being denoised. If those signals could not be rejected, the noise estimation would have been biased in the frequency domain. In addition, a smoothly decaying spatial kernel (k_s) was implemented to limit bias from spatially distant pixels. Subsequently, the two kernels (k_r and k_s) were combined to an unnormalized bilateral kernel. Finally, a discrete Fourier transform was performed to obtain the masked signal in the frequency domain (F_p), yielding the Fourier coefficients ($G_{i,p,f}$) for frequency f as follows:

$$G_{i,p,f} = \sum_{q \in N_p} g_{i,p,q} k_r\left(\frac{\left|g_{i,p,q}\right|^2}{T_i}\right) k_s\left(\frac{|q-p|^2}{S_i}\right) e^{-j\frac{2\pi}{2r+1} f \cdot (q-p)}$$

The imaginary number $j=\sqrt{-1}$ was used to avoid confusion with the iteration time i. Scale parameters T_i and S_i were obtained by deterministic annealing (DA) (21,22), as described previously:

$$T_i = \sigma^2 \gamma_r \alpha^{-i}$$
$$S_i = \sigma_s^2 \gamma_s \alpha^{i/2}$$

Where a^{-1} is the rate of an exponential decay, γ_r is a large initial scale factor, σ^2 is the noise variance of the noisy input y and σ^2 defines a reference standard deviation for the spatial kernel. Similar to the parameter γ_r of the range kernel, γ_s is a small initial scale factor for the scale σ_s of the spatial kernel.

After removing large amplitude signals, the medium amplitude signals were similarly masked in the frequency domain in order to obtain the remaining small amplitude noise. This procedure involved the use of another range kernel K to remove large Fourier coefficients. Finally, the noise was estimated by taking the center pixel following inverse Fourier transformation of the signal. To obtain this value, the Fourier slicing theorem was applied and averaged for all Fourier coefficients, as follows:

$$n_{i,p} = \frac{1}{(2r+1)^2} \sum_{f \in F_p} G_{i,p,f} K\left(\frac{\left|G_{i,p,f}\right|^2}{V_i}\right)$$

Where V_i is another scale parameter similar to the spatial domain. It is in this case the variance of the Fourier coefficients $G_{i,p,f}$, defined using the noise variance σ^2, as follows:

$$V_i = \sigma^2 \sum_{q \in N_p} k_r\left(\frac{\left|g_{i,p,q}\right|^2}{T_i}\right)^2 k_s\left(\frac{|q-p|^2}{S_i}\right)^2$$

Comparison of DDID method with NLM and BM3D. The DDID method proposed in the present study was compared with unbiased NLM (13) and BM3D (17). The parameters in the proposed method were empirically identified as mentioned

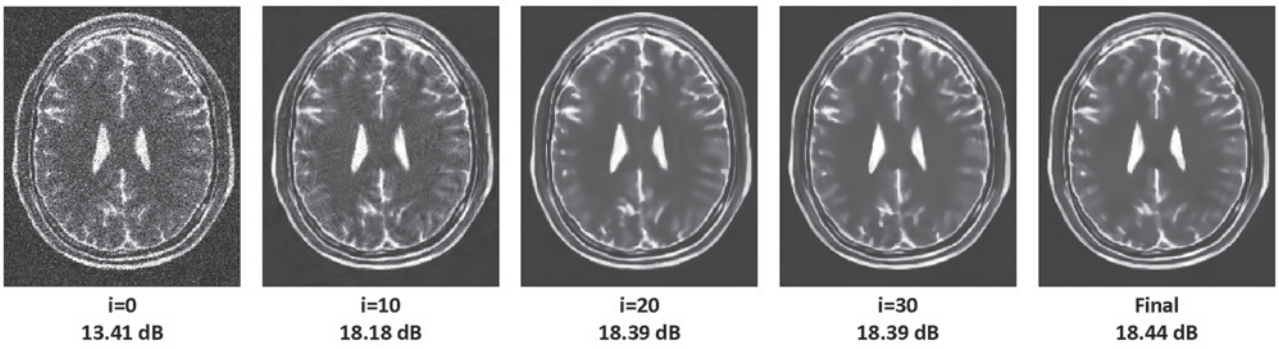

Figure 1. Denoising results following various iterations (0, 10, 20, 30 and 30). The Rician noise level was 15%. The second number denotes the increasing peak-signal-to-noise ratio.

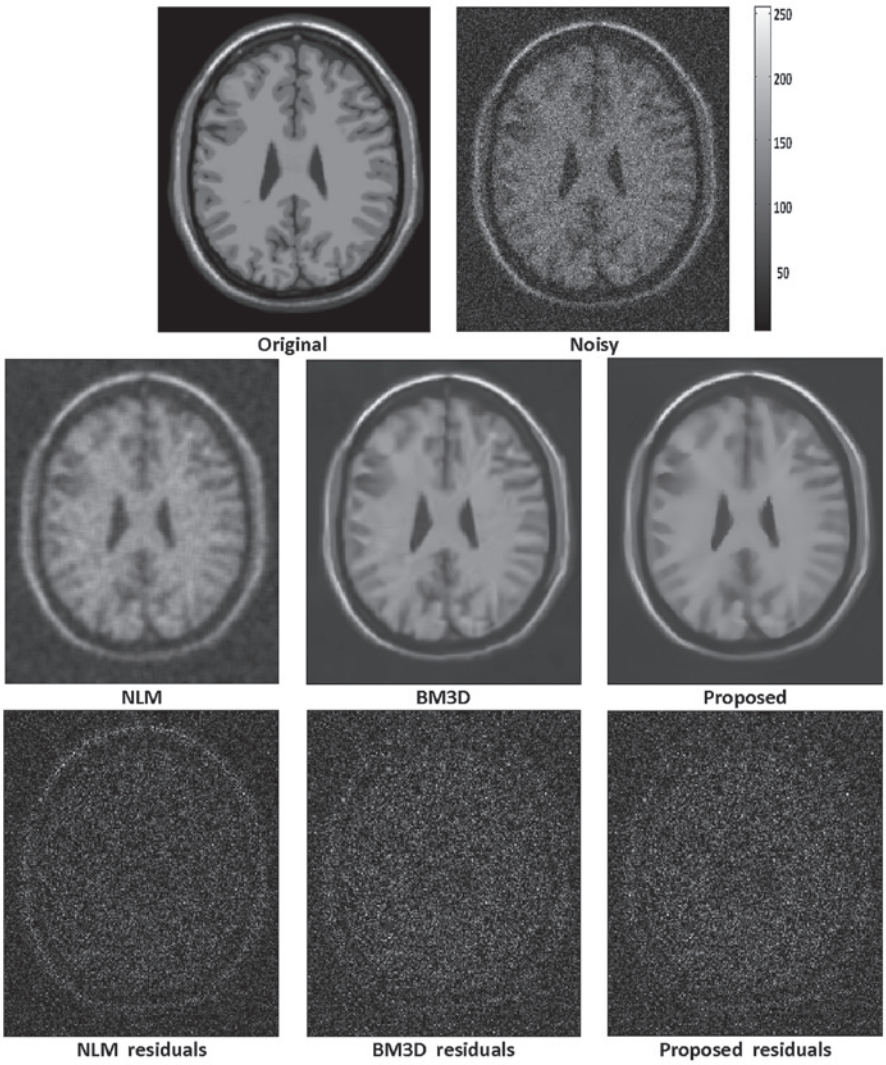

Figure 2. Example filtering results for an axial slice of the T1-weighted BrainWeb phantom (Rician noise level of 15%). The third row shows the absolute value of the image residuals for the various methods. NLM, nonlocal means filter; BM3D, block matching with 3D filtering.

above and were the same for all noise levels. A total of 30 iterations (N=30) and a window radius of 15 (r=15) was selected. The parameters for the NLM and BM3D methods were the optimal ones, as suggested in previous studies (13,17). All algorithms were processed on a desktop computer with an Intel Core™ i3 Processor and 4 GB random-access memory, and scripted in Matlab 2013a (http://uk.mathworks.com/products/new_products/release2013a.html).

Simulated and real datasets were used to evaluate the proposed method. The 3D simulated brain database BrainWeb (http://brainweb.bic.mni.mcgill.ca/brainweb/) was used for quantitative and qualitative comparisons in different modalities,

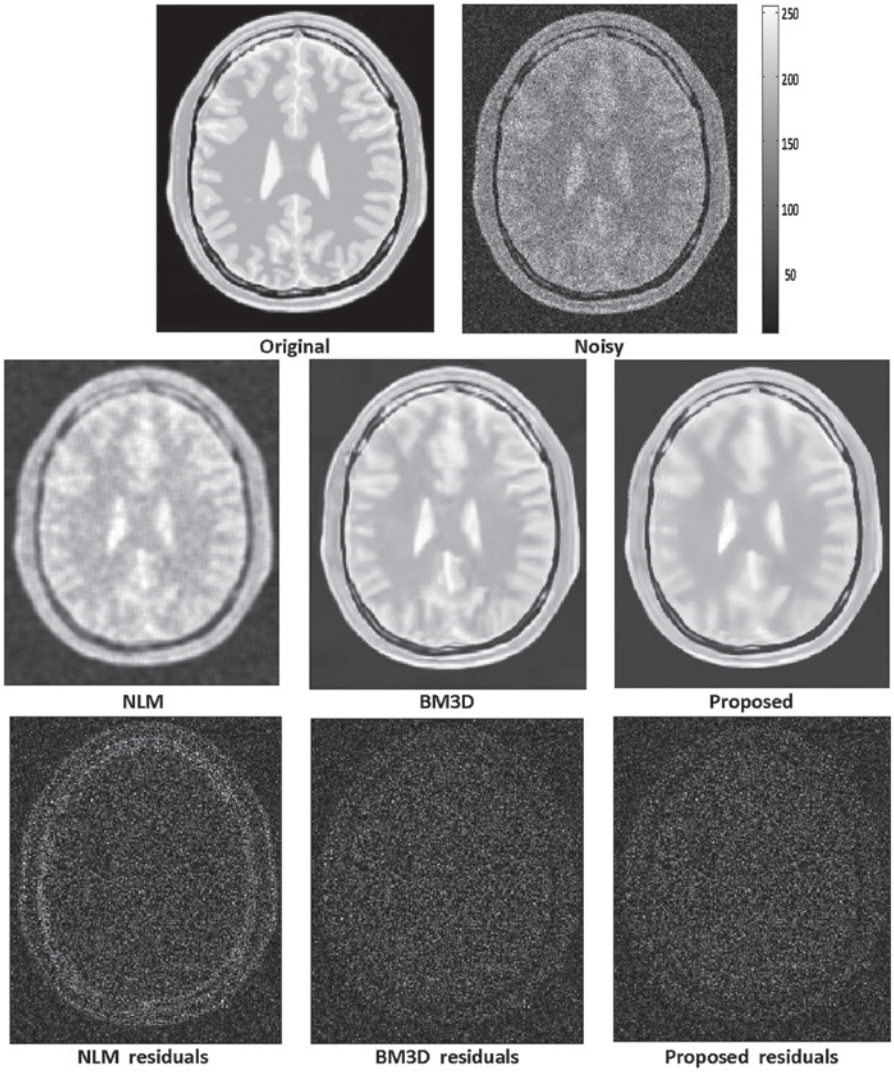

Figure 3. Example filtering results for an axial slice of the proton density-weighted BrainWeb phantom (Rician noise level of 15%). The third row shows the absolute value of the image residuals for the various methods. NLM, nonlocal means filter; BM3D, block matching with 3D filtering.

including T1-weighted (T1w), proton density (PD)-weighted and T2w, according to previous studies (23,24). All of the datasets were isotropic voxel with a resolution of 1 mm^3 and a spatial resolution of 181x217x181. With this phantom, the denoising results in the various iterations are presented in Fig. 1, and are qualitatively compared with NLM and BM3D in Figs. 2-4. The quantitative evaluation of these methods in the three modalities with varying levels of intensity (1-15% of maximum intensity) is presented in Table I. Three quality measures were used to evaluate the results: i) The root mean squared error (RMSE) metric, which is commonly used in image processing to analyze the differences between original and restored data; ii) the peak-to-noise ratio (PSNR), which measures the extent to which the noise has been suppressed; and iii) the structural similarity index (SSIM), which is a measure more consistent with the human visual system (25), as follows:

$$\mathrm{SSIM}(x,y)=\frac{(2\mu_x\mu_y)(2\sigma_{xy}+c_2)}{(\mu_x^2+\mu_y^2+c_1)(\sigma_x^2+\sigma_y^2+c_2)}$$

Where μ_x and μ_y are the mean values of images x and y, σ_x and σ_y are the standard deviation of images x and y, σ_{xy} is the covariance of x and y, x and $C_1=(k_1L)^2$ and $C_2=(k_2L)^2$ (where L is the dynamic range, $k_1=0.01$ and $k_2=0.03$). As suggested by Wang *et al* (25) in 2004, the SSIM was locally estimated using the Gaussian kernel of 3x3x3 voxels. Finally, the mean value of all estimations was used as a quality metric. For the sake of clarity, both measures were estimated only in the region of interest (ROI; head tissues) obtained by removing the background, as previously described (26).

The real 3D MRI dataset (spinal cord; 5 male and 5 female; age range, 20-26 years) was acquired using a Siemens 3T scanner (echo time=4.7 msec; repetition time=2,040 msec; inversion time=900 msec; voxel size=1.0x1.0x1.0 nm; image size=180x192x192 voxels; flip angle=8˚; Siemens AG, Munich, Germany). The Rician noise level was estimated to be ~3% of the maximum gray level intensity using the method proposed by Aja-Fernandez *et al* (8) in 2008. Since the original dataset was noisy already, only the restored images for the various methods are presented in Fig. 5. The second row is the enlarged images of the corresponding block in the first row. In addition to visual comparisons, the results of segmentation with a region growing algorithm (27) are also provided in the third

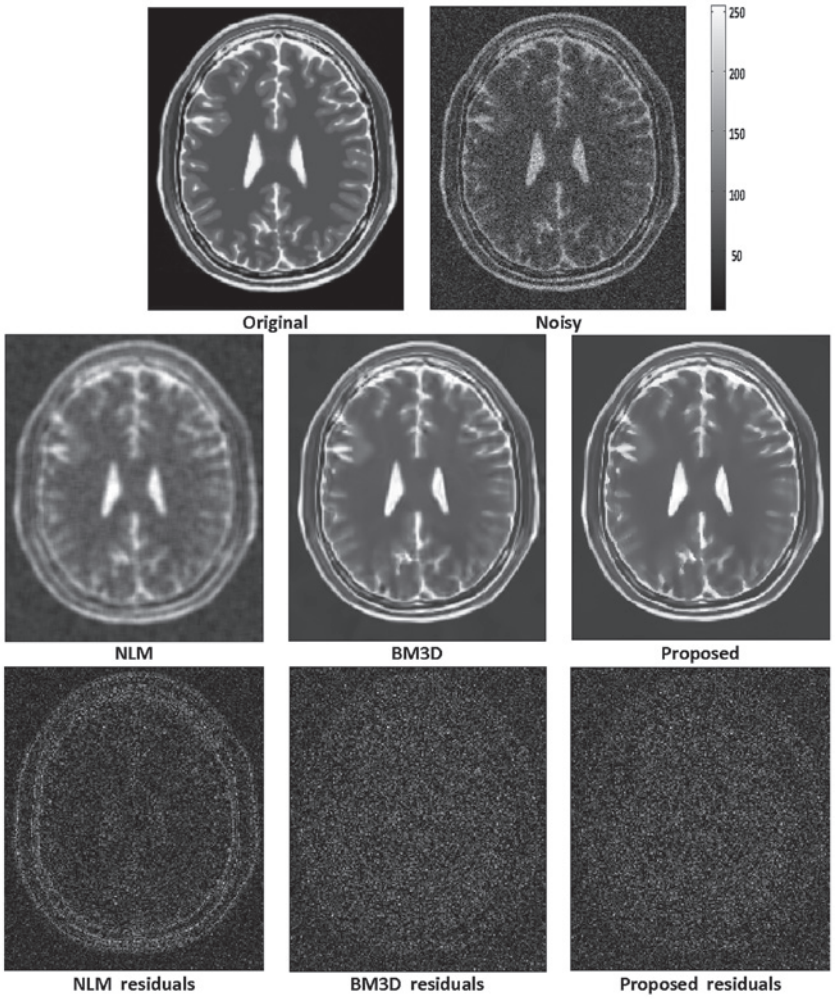

Figure 4. Example filtering results for an axial slice of the T2-weighted BrainWeb phantom (Rician noise level of 15%). The third row shows the absolute value of the image residuals for the various methods. NLM, nonlocal means filter; BM3D, block matching with 3D filtering.

row. The ROI was defined by dilating the seed for segmentation five times, and the resulting image was used as an ROI for quantitative analysis.

Results and Discussion

Evaluation of simulated datasets. Fig. 1 demonstrates that there were improvements in the visual quality and PSNR over time. During the initial 20 iterations, the PSNR markedly increased; however, it subsequently slowed down until convergence. This is not surprising, since the proposed method was able to effectively distinguish noise and large amplitude signals in the spatial domain, and then moderate the medium amplitude signal and noise in the frequency domain until convergence.

Figs. 2-4 present the denoised MRI images using the NLM, BM3D and proposed DDID methods in the T1w, PDw and T2w modalities, respectively. Only images with the highest noise intensities (15%) are presented in order to emphasize the differences among the algorithms. As can be observed, the proposed DDID method produced a visually more pleasant image, as compared with the NLM method, showing less grainy and more definite restored images. In addition, the denoised images generated by the proposed algorithm appeared clearer and less blurred in homogeneous areas (for example, T1w images in Fig. 2), and the boundaries were more clearly defined (for example, PD and T2w images in Figs. 3 and 4). These results may be due to the fact that the proposed method utilized information in both the spatial and transform domains to denoise MRI datasets, whereas the other methods were predominantly implemented in a single domain. Furthermore, the residual images in the third row demonstrated that the proposed and BM3D methods were superior, as compared with the NLM method, since there only minor anatomical information could be observed in their residual images, whereas the opposite occurred for NLM.

Table I presents a quantitative comparison of the three methods. The proposed method out-performed the NLM and BM3D methods and exhibited improvements over the NLM method. The NLM filter suffered from its lack of adaptation to particular properties of Rician noise (28). Conversely, BM3D is a state-of-the-art denoising method that has recently been developed (29); however, the proposed method was superior to the BM3D method in numerous cases. For example, the proposed method achieved better results at low noise levels for T1w data, and at high noise levels for PDw data. In addition, the best performance across the majority of noise levels was observed for the T2w data, which may be due to the high contrast on the T2w data.

Table I. RMSE, PSNR and SSIM of the compared methods for different MRI modalities and Rician noise levels.

	Noise level (%)							
Modality	1	3	5	7	9	11	13	15
T1w								
RMSE								
NLM	3.54	6.96	8.56	9.88	11.30	12.89	14.61	16.72
BM3D	1.68	3.66	5.27	6.81	8.58	10.54	12.53	15.00
Proposed	1.75	3.63	5.25	6.82	8.67	10.68	12.76	15.34
PSNR								
NLM	36.74	31.07	29.27	28.03	26.86	25.72	24.63	23.46
BM3D	43.40	36.65	33.48	31.26	29.26	27.47	25.97	24.40
Proposed	43.06	36.72	33.52	31.25	29.16	27.35	25.81	24.21
SSIM								
NLM	0.9700	0.9042	0.8666	0.8319	0.7968	0.7617	0.7275	0.6907
BM3D	0.9904	0.9632	0.9320	0.8993	0.8661	0.8326	0.8029	0.7697
Proposed	0.9908	0.9669	0.9356	0.9008	0.8638	0.8278	0.7967	0.7606
PDw								
RMSE								
NLM	4.63	7.96	10.70	13.00	14.77	16.17	17.34	18.58
BM3D	1.72	3.86	5.53	6.97	8.42	9.87	11.26	13.00
Proposed	1.78	3.94	5.61	7.01	8.41	9.76	11.15	12.80
PSNR								
NLM	34.81	30.11	27.55	25.85	24.74	23.95	23.35	22.75
BM3D	43.43	36.40	33.28	31.27	29.62	28.25	27.10	25.86
Proposed	43.14	36.22	33.16	31.22	29.64	28.35	27.19	25.98
SSIM								
NLM	0.9677	0.9051	0.8637	0.8259	0.7850	0.7467	0.7078	0.6731
BM3D	0.9898	0.9627	0.9334	0.9084	0.8768	0.8497	0.8201	0.7918
Proposed	0.9899	0.9633	0.9323	0.9038	0.8736	0.8472	0.8189	0.7949
T2w								
RMSE								
NLM	5.47	1073	15.31	18.07	19.89	21.32	22.74	24.31
BM3D	1.90	4.55	6.64	8.54	10.42	12.28	14.55	17.04
Proposed	1.94	4.62	6.62	8.40	10.29	12.20	14.45	16.90
PSNR								
NLM	33.37	27.52	24.43	22.99	22.16	21.55	20.99	20.42
BM3D	42.54	34.97	31.68	29.50	27.77	26.34	24.87	23.50
Proposed	42.36	34.84	31.71	29.64	27.88	26.40	24.94	23.57
SSIM								
NLM	0.9728	0.9075	0.8401	0.7856	0.7435	0.7088	0.6742	0.6463
BM3D	0.9915	0.9665	0.9403	0.9144	0.8885	0.8678	0.8406	0.8163
Proposed	0.9922	0.9694	0.9443	0.9187	0.8925	0.8707	0.8441	0.8201

RMSE, root mean squared error; PSNR, peak-to-noise ratio; SSIM, structural similarity index; MRI, magnetic resonance imaging; T1w, T1-weighted; PDw, proton density-weighted; T2-w, T2-weighted; NLM, nonlocal means filter; BM3D, block matching with 3D filtering.

Evaluation of clinical data. The consistency of the proposed method on spinal cord data was evaluated. As the original datasets already had noise, neither ideal residual images nor quantitative results could be obtained. As shown in Fig. 5, the proposed and BM3D methods exceeded NLM in terms of noise removal and sharpness. As compared with the other methods, the proposed method achieved a superior smoothing result, which was likely due to the robust estimation of noise

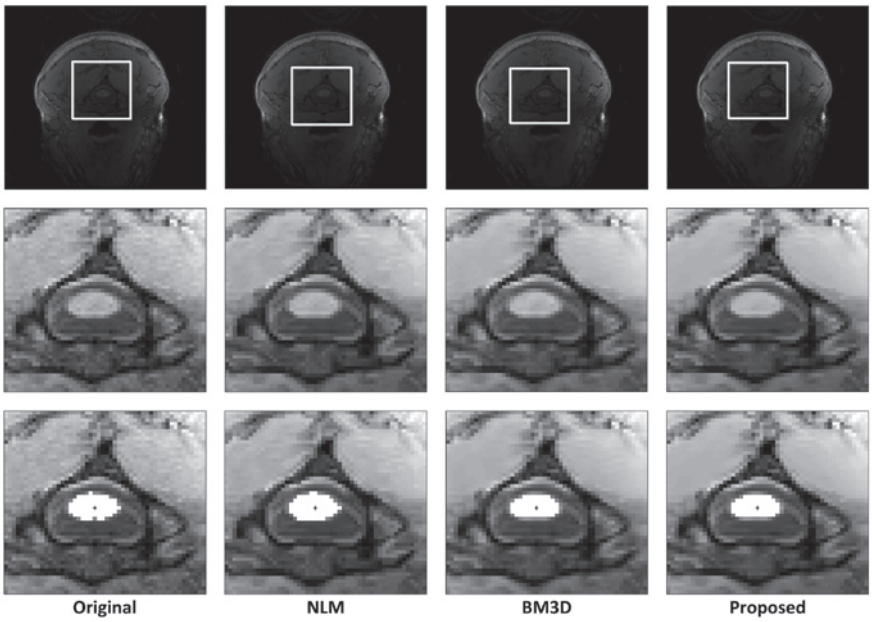

Figure 5. Example of *in vivo* MRI data (spinal cord). The first row is the original image, the second row is the enlarged part of block and the third row is the segmentation result (demonstrated in white). The black asterisk is the seed point. NLM, nonlocal means filter; BM3D, block matching with 3D filtering.

and effective differentiation of signal. Furthermore, upon close inspection of the central area of the ROI, the boundary of the spinal cord appeared to be clearer, which may have been due to the edge protection ability afforded by the DDID method. These results support the effects observed in the simulated images. The segmentation results in the proposed denoised MRI image exhibited smoother spinal cord contour, which appeared more physiologically realistic and may be beneficial to further applications.

In conclusion, the present study developed a novel DDID algorithm for denoising 3D MRI data that is assumed to be corrupted by Rician noise. This DDID method was implemented using a simple iterative filtering scheme that is beneficial for computation. In addition, Rician noise was robustly estimated using the algorithm, which unified the spatial and frequency domains. This accurate noise estimation was introduced by filtering iteratively, which ensured the plausible denoising result. Furthermore, the proposed method was implemented for both synthetic and *in vivo* MRI datasets, and was shown to achieve competitive results quantitatively and qualitatively.

Acknowledgements

The present study was supported by the National Basic Research Program of China (973 Program; grant no. 2014CB360506) and the National Natural Science Foundation of China (grant no. 81201158).

References

1. Wright GA: Magnetic resonance imaging. IEEE Signal Process Mag 14: 56-66, 1997.
2. Rodríguez AO: Principles of magnetic resonance imaging. Rev Mex Fis 50: 272-286, 2004.
3. López-Rubio E and Florentín-Núñez MN: Kernel regression based feature extraction for 3D MR image denoising. Medical Image Analysis 15: 498-513, 2011.
4. Mohan J, Krishnaveni V and Guo Y: A survey on the magnetic resonance image denoising methods. Biomedical Signal Process Control 9: 56-69, 2014.
5. Gudbjartsson H and Patz S: The Racian distribution of noisy MRI data. Magn Reson Med 34: 910-914, 1995.
6. Sijbers J, den Dekker AJ, Van Audekerke J, Verhoye M and Van Dyck D: Estimation of the noise in magnitude MR images. Magn Reson Imaging 16: 87-90, 1998.
7. Sijbers J, Poot D, den Dekker AJ and Pintjens W: Automatic estimation of the noise variance from the histogram of a magnetic resonance image. Phys Med Biol 52: 1335-1348, 2007.
8. Aja-Fernandez S, Alberola-Lopez C and Westin CF: Noise and signal estimation in magnitude MRI and Rician distributed images: A LMMSE approach. IEEE Trans Image Process 17: 1383-1398, 2008.
9. Aja-Fernandez S, Niethammer M, Kubicki M, Shenton ME and Westin CF: Restoration of DWI data using a Rician LMMSE estimator. IEEE Trans Med Imaging 27: 1389-1403, 2008.
10. Martin-Fernandez M, Muñoz-Moreno E, Cammoun L, Thiran JP, Westin CF and Alberola-López C: Sequential anisotropic multichannel Wiener filtering with Rician bias correction applied to 3D regularization DWI data. Med Image Anal 13: 19-35, 2009.
11. McVeigh ER, Henkelman RM and Bronskill MJ: Noise and filteration in magnetic resonance imaging. Med Phys 12: 586-591, 1985.
12. Perona P and Malik J: Scale-space and edge detection using anisotropic diffusion. IEEE Trans Pattern Anal Mach Intell 12: 629-639, 1990.
13. Buades A, Coll B and Morel JM: A review of image denoising algorithms, with a new one. Multiscale Model Simul 4: 490-530, 2005.
14. Manjón JV, Carbonell-Caballero J, Lull JJ, García-Martí G, Martí-Bonmatí L and Robles M: MRI denoising using non-local means. Med Image Anal 12: 514-523, 2008.
15. Wu X, Liu S, Wu M, Sun H, Zhou J, Gong Q and Ding Z: Nonlocal denoising using anisotropic structure tensor for 3D MRI. Med Phys 40: 101904, 2013.
16. Pizurica A, Philips W, Lemahieu I and Acheroy M: A versatile wavelet domain noise filtration technique for medical imaging. IEEE Trans Med Imaging 22: 323-331, 2003.
17. Foi A, Katkovnik V and Egiazarian K: Pointwise shape-adaptive DCT for high-quality denoising and deblocking of grayscale and color images. IEEE Trans Image Process 16: 1395-1411, 2007.
18. Dabov K, Foi A, Katkovnik V and Egiazarian K: Image denoising by sparse 3D transform-domain collaborative filtering. IEEE Trans Image Process 16: 2080-2095, 2007.
19. Knaus C and Zwicker M: Progressive image denoising. IEEE Trans Image Process 23: 3114-3125, 2014.

20. Knaus C and Zwicker M: Dual-domain image denoising. In: 2013 IEEE International Conference on Image Processing. Melbourne, VIC, pp440-444, 2013.
21. Li SZ: Robustizing robust M-estimation using deterministic annealing. Pattern Recognit 29: 159-166, 1996.
22. Fruhwirth R and Waltenberger W: Redescending M-estimators and deterministic annealing, with application to robust regression and tail index estimation. Aust J Stat 37: 301-317, 2010.
23. Collins DL, Zijdenbos AP, Kollokian V, Sled JG, Kabani NJ, Holmes CJ and Evans AC: Design and construction of a realistic digital brain phantom. IEEE Trans Med Imaging 17: 463-468, 1998.
24. Kwan RK, Evans AC and Pike GB: MRI simulation-based evaluation of image-processing and classification methods. IEEE Trans Med Imaging 18: 1085-1097, 1999.
25. Wang Z, Bovik AC, Sheikh HR and Simoncelli EP: Image quality assessment: From error visibility to structural similarity. IEEE Trans Image Process 13: 600-612, 2004.
26. Liu T, Khalidov I, de Rochefort L,Spincemaille P, Liu J, Tsiouris AJ and Wang Y: A novel background field removal method for MRI using projection onto dipole fields (PDF). Nmr Biomed 24: 1129-1136, 2011.
27. Gonzalez RC and Woods RE: Digital Image Processing. 2nd edition. Prentice Hall, Upper Saddle River, NJ, 2002.
28. Manjón JV, Coupé P, Buades A, Louis Collins D and Robles M: New methods for MRI denoising based on sparseness and self-similarity. Med Image Anal 16: 18-27, 2012.
29. Levin A, Nadler B, Durand F and Freeman WT: Patch complexity, finite pixel correlations and optimal denoising. Computer Vision ECCV 2012: 73-86, 2012.